

# A Measurement of $\psi(2S)$ Resonance Parameters

(BES Collaboration)

J. Z. Bai<sup>1</sup>, Y. Ban<sup>10</sup>, J. G. Bian<sup>1</sup>, I. Blum<sup>18</sup>, X. Cai<sup>1</sup>, J. F. Chang<sup>1</sup>, H. F. Chen<sup>17</sup>, H. S. Chen<sup>1</sup>, J. Chen<sup>4</sup>, Jie Chen<sup>9</sup>, J. C. Chen<sup>1</sup>, Y. B. Chen<sup>1</sup>, S. P. Chi<sup>1</sup>, Y. P. Chu<sup>1</sup>, X. Z. Cui<sup>1</sup>, Y. S. Dai<sup>20</sup>, L. Y. Dong<sup>1</sup>, Z. Z. Du<sup>1</sup>, W. Dunwoodie<sup>14</sup>, J. Fang<sup>1</sup>, S. S. Fang<sup>1</sup>, H. Y. Fu<sup>1</sup>, L. P. Fu<sup>7</sup>, C. S. Gao<sup>1</sup>, Y. N. Gao<sup>15</sup>, M. Y. Gong<sup>1</sup>, P. Gratton<sup>18</sup>, S. D. Gu<sup>1</sup>, Y. N. Guo<sup>1</sup>, Y. Q. Guo<sup>1</sup>, Z. J. Guo<sup>3</sup>, S. W. Han<sup>1</sup>, F. A. Harris<sup>16</sup>, J. He<sup>1</sup>, K. L. He<sup>1</sup>, M. He<sup>11</sup>, X. He<sup>1</sup>, Y. K. Heng<sup>1</sup>, T. Hong<sup>1</sup>, H. M. Hu<sup>1</sup>, T. Hu<sup>1</sup>, G. S. Huang<sup>1</sup>, X. P. Huang<sup>1</sup>, J. M. Izen<sup>18</sup>, X. B. Ji<sup>11</sup>, C. H. Jiang<sup>1</sup>, X. S. Jiang<sup>1</sup>, D. P. Jin<sup>1</sup>, S. Jin<sup>1</sup>, Y. Jin<sup>1</sup>, B. D. Jones<sup>18</sup>, Z. J. Ke<sup>1</sup>, D. Kong<sup>16</sup>, Y. F. Lai<sup>1</sup>, G. Li<sup>1</sup>, H. H. Li<sup>6</sup>, J. Li<sup>1</sup>, J. C. Li<sup>1</sup>, Q. J. Li<sup>1</sup>, R. Y. Li<sup>1</sup>, W. Li<sup>1</sup>, W. G. Li<sup>1</sup>, X. Q. Li<sup>9</sup>, C. F. Liu<sup>19</sup>, F. Liu<sup>6</sup>, H. M. Liu<sup>1</sup>, J. P. Liu<sup>19</sup>, R. G. Liu<sup>1</sup>, T. R. Liu<sup>1</sup>, Y. Liu<sup>1</sup>, Z. A. Liu<sup>1</sup>, Z. X. Liu<sup>1</sup>, X. C. Lou<sup>18</sup>, B. Lowery<sup>18</sup>, G. R. Lu<sup>5</sup>, F. Lu<sup>1</sup>, H. J. Lu<sup>17</sup>, J. G. Lu<sup>1</sup>, Z. J. Lu<sup>1</sup>, X. L. Luo<sup>1</sup>, E. C. Ma<sup>1</sup>, F. C. Ma<sup>8</sup>, J. M. Ma<sup>1</sup>, R. Malchow<sup>4</sup>, Z. P. Mao<sup>1</sup>, X. C. Meng<sup>1</sup>, X. H. Mo<sup>3</sup>, J. Nie<sup>1</sup>, Z. D. Nie<sup>1</sup>, S. L. Olsen<sup>16</sup>, D. Paluselli<sup>16</sup>, L. J. Pan<sup>16</sup>, J. Panetta<sup>2</sup>, H. P. Peng<sup>17</sup>, F. Porter<sup>2</sup>, N. D. Qi<sup>1</sup>, C. D. Qian<sup>12</sup>, J. F. Qiu<sup>1</sup>, G. Rong<sup>1</sup>, D. L. Shen<sup>1</sup>, H. Shen<sup>1</sup>, X. Y. Shen<sup>1</sup>, H. Y. Sheng<sup>1</sup>, F. Shi<sup>1</sup>, J. Standifird<sup>18</sup>, H. S. Sun<sup>1</sup>, S. S. Sun<sup>17</sup>, Y. Z. Sun<sup>1</sup>, X. Tang<sup>1</sup>, D. Tian<sup>1</sup>, W. Toki<sup>4</sup>, G. L. Tong<sup>1</sup>, G. S. Varner<sup>16</sup>, J. Wang<sup>1</sup>, J. Z. Wang<sup>1</sup>, L. Wang<sup>1</sup>, L. S. Wang<sup>1</sup>, M. Wang<sup>1</sup>, Meng Wang<sup>1</sup>, P. Wang<sup>1</sup>, P. L. Wang<sup>1</sup>, W. F. Wang<sup>11</sup>, Y. F. Wang<sup>1</sup>, Y. Y. Wang<sup>1</sup>, Z. Wang<sup>1</sup>, Zheng Wang<sup>1</sup>, Z. Y. Wang<sup>3</sup>, M. Weaver<sup>2</sup>, C. L. Wei<sup>1</sup>, N. Wu<sup>1</sup>, X. M. Xia<sup>1</sup>, X. X. Xie<sup>1</sup>, G. F. Xu<sup>1</sup>, Y. Xu<sup>1</sup>, S. T. Xue<sup>1</sup>, M. L. Yan<sup>17</sup>, W. B. Yan<sup>1</sup>, C. Y. Yang<sup>1</sup>, G. A. Yang<sup>1</sup>, H. X. Yang<sup>15</sup>, M. H. Ye<sup>3</sup>, S. W. Ye<sup>17</sup>, Y. X. Ye<sup>17</sup>, J. Ying<sup>10</sup>, C. S. Yu<sup>1</sup>, G. W. Yu<sup>1</sup>, C. Z. Yuan<sup>1</sup>, J. M. Yuan<sup>20</sup>, Y. Yuan<sup>1</sup>, Q. Yue<sup>1</sup>, Y. Zeng<sup>7</sup>, B. X. Zhang<sup>1</sup>, B. Y. Zhang<sup>1</sup>, C. C. Zhang<sup>1</sup>, D. H. Zhang<sup>1</sup>, H. Y. Zhang<sup>1</sup>, J. Zhang<sup>1</sup>, J. W. Zhang<sup>1</sup>, L. Zhang<sup>1</sup>, L. S. Zhang<sup>1</sup>, Q. J. Zhang<sup>1</sup>, S. Q. Zhang<sup>1</sup>, X. Y. Zhang<sup>11</sup>, Y. Y. Zhang<sup>1</sup>, Yiyun Zhang<sup>13</sup>, Z. P. Zhang<sup>17</sup>, D. X. Zhao<sup>1</sup>, Jiawei Zhao<sup>17</sup>, J. W. Zhao<sup>1</sup>, P. P. Zhao<sup>1</sup>, W. R. Zhao<sup>1</sup>, Y. B. Zhao<sup>1</sup>, Z. G. Zhao<sup>1†</sup>, J. P. Zheng<sup>1</sup>, L. S. Zheng<sup>1</sup>, Z. P. Zheng<sup>1</sup>, X. C. Zhong<sup>1</sup>, B. Q. Zhou<sup>1</sup>, G. M. Zhou<sup>1</sup>, L. Zhou<sup>1</sup>, K. J. Zhu<sup>1</sup>, Q. M. Zhu<sup>1</sup>, Y. C. Zhu<sup>1</sup>, Y. S. Zhu<sup>1</sup>, Z. A. Zhu<sup>1</sup>, B. A. Zhuang<sup>1</sup>, B. S. Zou<sup>1</sup>.

<sup>1</sup> Institute of High Energy Physics, Beijing 100039, People's Republic of China

<sup>2</sup> California Institute of Technology, Pasadena, California 91125

<sup>3</sup> China Center of Advanced Science and Technology, Beijing 100080, People's Republic of China

<sup>4</sup> Colorado State University, Fort Collins, Colorado 80523

<sup>5</sup> Henan Normal University, Xinxiang 453002, People's Republic of China

<sup>6</sup> Huazhong Normal University, Wuhan 430079, People's Republic of China

<sup>7</sup> Hunan University, Changsha 410082, People's Republic of China

<sup>8</sup> Liaoning University, Shenyang 110036, People's Republic of China

<sup>9</sup> Nankai University, Tianjin 300071, People's Republic of China

<sup>10</sup> Peking University, Beijing 100871, People's Republic of China

<sup>11</sup> Shandong University, Jinan 250100, People's Republic of China

<sup>12</sup> Shanghai Jiaotong University, Shanghai 200030, People's Republic of China

<sup>13</sup> Sichuan University, Chengdu 610064, People's Republic of China

<sup>14</sup> Stanford Linear Accelerator Center, Stanford, California 94309

<sup>15</sup> Tsinghua University, Beijing 100084, People's Republic of China

<sup>16</sup> University of Hawaii, Honolulu, Hawaii 96822

<sup>17</sup> University of Science and Technology of China, Hefei 230026, People's Republic of China

<sup>18</sup> University of Texas at Dallas, Richardson, Texas 75083-0688

<sup>19</sup> Wuhan University, Wuhan 430072, People's Republic of China

<sup>20</sup> Zhejiang University, Hangzhou 310028, People's Republic of China

<sup>†</sup> Visiting professor to University of Michigan, Ann Arbor, MI 48109 USA

Cross sections for  $e^+e^- \rightarrow$  hadrons,  $\pi^+\pi^-J/\psi$ , and  $\mu^+\mu^-$  have been measured in the vicinity of the  $\psi(2S)$  resonance using the BESII detector operated at the BEPC. The  $\psi(2S)$  total width; partial widths to hadrons,  $\pi^+\pi^-J/\psi$ , leptons; and corresponding branching fractions have been determined to be  $\Gamma_t = 264 \pm 27$  keV;  $\Gamma_h = 258 \pm 26$  keV,  $\Gamma_{\pi^+\pi^-J/\psi} = 85.4 \pm 8.7$  keV, and  $\Gamma_l = 2.44 \pm 0.21$  keV; and  $B_h = (97.79 \pm 0.15)\%$ ,  $B_{\pi^+\pi^-J/\psi} = (32.3 \pm 1.4)\%$ , and  $B_l = (0.93 \pm 0.08)\%$ , respectively.

## 1. Introduction

Since the discovery of the  $\psi(2S)$  in 1974 [1], measurements of its total width ( $\Gamma_t$ ), and partial decay widths into hadrons ( $\Gamma_h$ ),  $\pi^+\pi^-J/\psi$  ( $\Gamma_{\pi^+\pi^-J/\psi}$ ), and  $l^+l^-$  ( $\Gamma_l$ ), and the corresponding branching fractions,  $B_h$ ,  $B_{\pi^+\pi^-J/\psi}$ , and  $B_l$ , have been carried out [2–10]. The results of these experiments differ on both decay widths and branching fractions. The parameters are of particular interest because, for instance,  $\psi(2S) \rightarrow l^+l^-$  is used in reconstructing  $B$  mesons for  $CP$  violation measurements [11], and  $\psi(2S) \rightarrow \pi^+\pi^-J/\psi$  is often used to determine the total number of  $\psi(2S)$  events in  $\psi(2S)$  branching fraction measurements due to its large branching fraction and straightforward detection. Therefore, it is important to measure these decay widths and branching fractions with better accuracy.

Twenty four center-of-mass energy points were scanned in the vicinity of the  $\psi(2S)$  peak ranging from 3.67 GeV to 3.71 GeV. The data were collected with the BESII (BEijing Spectrometer) detector at the BEPC (BEijing Electron Positron Collider) storage ring. The BESII detector is described in detail in Ref. [12]. In addition, separated-beam data were taken at the first and the last points for background studies. The total integrated luminosity was  $1149 \text{ nb}^{-1}$ .

## 2. Event selection

The following four reactions are studied:

$$\begin{aligned} e^+e^- &\rightarrow e^+e^- \quad , \\ e^+e^- &\rightarrow \mu^+\mu^- \quad , \\ e^+e^- &\rightarrow \pi^+\pi^-J/\psi \quad , \\ e^+e^- &\rightarrow \text{hadrons} \quad . \end{aligned}$$

For the selection of lepton-pair final states, two charged tracks with total charge zero are required. For  $\mu^+\mu^-$  events, the acollinearity must be less than 10 degrees. In addition, in order to suppress cosmic ray background, the time-of-flight measurements of the two muon-candidates must satisfy  $\sqrt{(t_1 - 5)^2 + (t_2 - 5)^2} < 4.5(\text{ns})$ , as shown in Fig. 1. Further, the Muon Counter hit information is used to identify di-muon events from other back-to-back two-prong final states, and this re-

quires  $|\cos\theta_\mu| \leq 0.65$  due to the limited solid angle coverage.

To separate electrons from muons and hadrons, the energies deposited by the two tracks in the Barrel Shower Counter (BSC) must satisfy  $\sqrt{(\tilde{E}_{dep1} - 1)^2 + (\tilde{E}_{dep2} - 1)^2} < 0.65$ , where  $\tilde{E}_{dep} = \frac{E_{dep}}{E_{beam}}$  is the normalized energy deposited. We also require  $|\cos\theta_e| \leq 0.72$ , and because the Monte Carlo simulation does not model the energy deposited well in the rib region of the BSC, an additional cut is applied on the  $z$ -coordinate of the first hit layer:  $0.03 < |z_{sc}| < 0.85$  or  $|z_{sc}| > 0.95 \text{ m}$ .

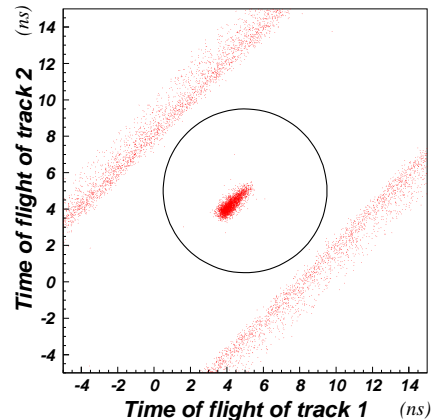


Figure 1. Times of flight for  $\mu$ -pairs. The diagonal bands are due to cosmic ray events. Good events, which cluster at the center of the plot are selected with the circle cut shown.

A potential source of background is lepton-pairs coming from  $\psi(2S) \rightarrow XJ/\psi$ ,  $J/\psi \rightarrow l^+l^-$ . To eliminate this background, we make cuts on the track momenta, as shown in Fig. 2 [13].

Using the above criteria to select  $\mu^+\mu^-$  and  $e^+e^-$  events, we have compared various distributions with Monte Carlo distributions. Good agreement is found, as illustrated, for example, in Fig. 3.

For hadron event selection, we are guided by

our R-scan experience [14,15]. There is no particular event topology to require; instead we make cuts to reject major backgrounds: cosmic rays, beam-associated background, two-photon processes ( $\gamma^*\gamma^*$ ), mis-identified ‘‘hadron’’ events from QED processes of  $e^+e^- \rightarrow l^+l^-$ ,  $l = e, \mu, \tau$ , and  $e^+e^- \rightarrow \gamma\gamma$  followed by  $\gamma$  conversion, etc. Events with at least two well reconstructed charged tracks within  $|\cos\theta| \leq 0.8$  are selected. The total energy deposited by an event in the BSC ( $E_{sum}$ ) is required to be larger than  $0.36E_{beam}$ , in order to suppress contamination from two-photon processes and beam associated background. Events with all tracks pointing to the same hemisphere in the  $z$  direction are removed to suppress beam-associated background. For two-prong events, two additional cuts are applied to eliminate possible lepton pair background. The number of photons must be greater than one, and the acollinearity between two charged tracks,  $\alpha_{Acol}$ , must be greater than 10 degrees. A comparison between data and Monte Carlo samples satisfied the foregoing selection criteria is shown in Fig. 4.

The background from  $\tau^+\tau^-$  decay is difficult to distinguish from direct hadronic decay events, so the contribution from this source,  $N_{\tau^+\tau^-}$ , is estimated using  $N_{\tau\tau} = L \cdot (\varepsilon_{\tau\tau} \cdot \sigma_{\tau\tau})$ , where  $L$  is the integrated luminosity at each energy point,  $\sigma_{\tau\tau}$  the QED production cross section at this energy point, and  $\varepsilon_{\tau\tau}$  the acceptance of our hadron event selection criteria for  $\tau^+\tau^-$  events. This is subtracted from the observed number of hadron events. A similar subtraction is performed for the other surviving backgrounds, such as  $e^+e^- \rightarrow e^+e^-, \mu^+\mu^-, \gamma\gamma$ , and the two-photon process ( $\gamma^*\gamma^*$ ). Therefore, the corrected number of hadron events,  $N_h^{obs}$ , is

$$N_h^{obs} = N_h - N_{\tau\tau} - N_{ee} - N_{\mu\mu} - N_{\gamma\gamma} - N_{\gamma^*\gamma^*}$$

where  $N_h$  is the number of events that satisfy the hadron event selection cuts. The numbers of various backgrounds are given in Table 1.

For the selection of  $\psi(2S) \rightarrow \pi^+\pi^- J/\psi$  events, we select a pair of low energy pions and determine the mass recoiling against these two pions,  $m_{recoil}$ , which shows a strong  $J/\psi$  peak, corresponding to the decay  $\psi(2S) \rightarrow \pi^+\pi^- J/\psi$ . The

Table 1

Estimated numbers of hadron event backgrounds.

$E_{cm}$ (GeV)	Background events				
	$N_{\tau\tau}$	$N_{ee}$	$N_{\mu\mu}$	$N_{\gamma\gamma}$	$N_{\gamma^*\gamma^*}$
3.6668	20.79	12.16	0.22	0.80	1.45
3.6719	20.36	11.91	0.21	0.78	1.42
3.6750	20.15	11.79	0.21	0.78	1.41
3.6781	20.72	12.12	0.22	0.80	1.46
3.6801	20.58	12.04	0.21	0.79	1.45
3.6809	22.18	12.98	0.23	0.85	1.56
3.6820	20.80	12.17	0.22	0.80	1.46
3.6828	20.60	12.05	0.21	0.79	1.45
3.6832	20.66	12.09	0.22	0.80	1.46
3.6836	21.52	12.59	0.22	0.83	1.52
3.6844	20.61	12.06	0.22	0.79	1.45
3.6850	21.44	12.54	0.22	0.83	1.51
3.6855	19.98	11.69	0.21	0.77	1.41
3.6863	19.79	11.58	0.21	0.76	1.40
3.6867	19.92	11.66	0.21	0.77	1.41
3.6875	19.88	11.63	0.21	0.77	1.41
3.6882	20.42	11.95	0.21	0.79	1.44
3.6886	20.19	11.81	0.21	0.78	1.43
3.6893	25.36	14.84	0.26	0.98	1.79
3.6908	20.97	12.27	0.22	0.81	1.49
3.6939	23.11	13.52	0.24	0.89	1.64
3.6979	22.38	13.09	0.23	0.86	1.59
3.7017	21.89	12.81	0.23	0.84	1.56
3.7068	22.56	13.20	0.24	0.87	1.62

$m_{recoil}$  distribution is fitted with a signal shape plus polynomial background to obtain the number of  $\psi(2S) \rightarrow \pi^+\pi^- J/\psi$  events at each energy point. The very clean  $\psi(2S) \rightarrow \pi^+\pi^- J/\psi$ ,  $J/\psi \rightarrow l^+l^-$  channel is used to determine the signal shape. The inclusive  $m_{recoil}$  distribution for all 24 energy points combined is shown in Fig. 5. For more detail, see Ref. [16]. The numbers of events selected for the four final states at the 24 energies are listed in Table 2.

### 3. Acceptance

The acceptance is the product of the trigger efficiency and the reconstruction-selection effi-

Table 2  
Numbers of events selected.

$E_{cm}$ (GeV)	Selected number of events			
	$N_{ee}^{obs}$	$N_{\mu\mu}^{obs}$	$N_h^{obs}$	$N_{\pi^+\pi^-J/\psi}^{obs}$
3.6668	1789	110	385	7.2
3.6719	1752	92	389	10.2
3.6750	1734	124	391	22.3
3.6781	1783	102	437	0.0
3.6801	1771	66	485	12.8
3.6809	1909	104	588	14.2
3.6820	1790	91	764	75.0
3.6828	1773	86	1538	181.0
3.6832	1778	69	2662	426.1
3.6836	1852	79	4178	668.0
3.6844	1774	92	8169	1508.0
3.6850	1845	128	14684	2660.8
3.6855	1720	140	15073	2758.1
3.6863	1703	191	15621	2902.6
3.6867	1715	176	14980	2572.0
3.6875	1711	161	11658	2201.8
3.6882	1758	175	7047	1245.1
3.6886	1738	125	4960	868.9
3.6893	2183	188	3964	707.4
3.6908	1805	113	1897	269.0
3.6939	1989	97	1318	128.8
3.6979	1926	132	1029	82.6
3.7017	1884	118	876	77.2
3.7068	1942	120	729	26.5
sum	43624	2879	113823	19425.4

ciency. The triggers are the same as those used in our  $R$  scan experiment [14]. The trigger efficiencies, measured by comparing the responses to different trigger requirements in special runs taken at the  $J/\psi$  resonance, are determined to be 1.000, 0.994 and 0.998 for  $e^+e^-$ ,  $\mu^+\mu^-$  and hadronic events respectively, with an uncertainty of 0.005.

Different generators are used to determine the reconstruction-selection efficiencies. For  $e^+e^-$  and  $\mu^+\mu^-$  final states, the efficiencies for QED processes are determined in simulations with the BHABHA and MUPAIR generators [17]. The resonance  $e^+e^-$  and  $\mu^+\mu^-$  efficiencies are determined using the generator V2LL, adapted from

MUPAIR, with the initial state radiative corrections removed. For the hadronic processes, an event generator for charmonium inclusive decay [18] is used to obtain the efficiency for the resonance portion, and the JETSET string fragmentation algorithm with parameters modified to fit the experimental data in the BEPC energy region [19] is used to compute the efficiency for the continuum portion. For the  $\pi^+\pi^-J/\psi$  acceptance, a phase space Monte Carlo program, modified to give the correct dipion mass and angular distributions [20], is used.

Table 3

Acceptances for continuum,  $A^c$ , and the resonance,  $A^r$ .

final state	$e^+e^-$	$\mu^+\mu^-$	$had$	$\pi^+\pi^-J/\psi$
$A^c$ (%)	72.4	37.1	74.5	–
$\delta A^c/A^c$ (%)	3.2	5.0	7.1	–
$A^r$ (%)	76.4	41.9	77.1	43.4
$\delta A^r/A^r$ (%)	8.5	4.7	2.2	3.4

The acceptances of the four final states for continuum ( $A^c$ ) and resonance ( $A^r$ ) processes, together with their relative errors, are listed in Table 3. Here the acceptance for the  $e^+e^-$  final state in the table applies to events within a restricted solid angle ( $|\cos\theta_e| \leq 0.72$ ), whereas those of the hadron and dimuon final states cover all solid angles. The acceptance error includes the uncertainties estimated by varying selection cuts and using different selection methods and Monte Carlo models.

#### 4. Fit of observed cross sections and results

The  $e^+e^- \rightarrow$  hadrons,  $\pi^+\pi^-J/\psi$ ,  $e^+e^-$ , and  $\mu^+\mu^-$  events at the 24 scan points are fitted simultaneously to obtain the partial widths of  $\psi(2S)$  to hadrons,  $\pi^+\pi^-J/\psi$ , and  $\mu^+\mu^-$  final states. The total width is assumed to be the sum of four partial widths,  $\Gamma_t = \Gamma_h + \Gamma_\mu + \Gamma_e + \Gamma_\tau$ , and lepton universality is assumed\*,  $\Gamma_e = \Gamma_\mu =$

\*BES collaboration has measured the branching fraction of  $\psi(2S)$  decay into  $\tau^+\tau^-$ . This value along with those

$\Gamma_\tau/0.38847$ . A likelihood function is constructed [22]. Two kinds of correlations are taken into consideration in the fitting formula: one is the correlation between different channels at the same energy point, because the same luminosity is used to determine the cross sections at each energy; the other is the correlation between different energy points for each channel, due to the acceptance uncertainty being the same for all scan points. The MINUIT package [23] for maximization is used to give the best estimates for  $\psi(2S)$  parameters and their uncertainties. The theoretical cross section used in the fit for the hadron channel uses a Breit-Wigner amplitude and a non-resonant direct-channel amplitude plus a  $J/\psi$  resonance “tail” cross section, as determined by a previous BES  $J/\psi$  scan experiment [24]. The contributions from  $\psi(2S)$  decay into  $e^+e^-$ ,  $\mu^+\mu^-$ ,  $\tau^+\tau^-$  final states mis-identified as hadron events have been taken into account by correcting the resonant hadron event acceptance<sup>†</sup>. For the  $\pi^+\pi^-J/\psi$  final state, only a resonant Breit-Wigner amplitude is considered. In the  $\mu^+\mu^-$  channel, the  $\psi(2S)$  resonant term, QED term, and their interference are included. The radiative corrections to these three processes are taken into account by the formulation of Refs. [25] and [26]. For the  $e^+e^-$  final state, where the QED  $t$ -channel photon exchange also contributes, a theoretical cross section including radiative corrections is derived using the method of Ref. [27]. The effects on lepton-pair final state cross sections coming from vacuum polarization are also taken into consideration [28]; while for hadronic final states, the vacuum polarization is absorbed into the definition of  $\Gamma_{ee}$ , that is

$$\Gamma_{exp}(\psi(2S) \rightarrow e^+e^-) = \Gamma_0(\psi(2S) \rightarrow e^+e^-) \cdot \frac{1}{|1 - \prod (M_{\psi(2S)}^2)|^2},$$

where  $\Gamma_{exp}$  is the experimental width,  $\Gamma_0$  the low-order in  $\alpha$  width, and  $\prod$  the order  $\alpha$  vacuum

of the branching fractions in  $e^+e^-$  and  $\mu^+\mu^-$ , satisfies the relation predicted by the sequential lepton hypothesis within errors[21].

<sup>†</sup>The contaminations from QED processes  $e^+e^- \rightarrow l+l^-$  have been already subtracted, see section 2.

polarization [29]. The theoretical cross sections are convoluted with the energy distribution of the colliding beams, which is treated as Gaussian. The following parameters are allowed to vary in the fit: the  $\psi(2S)$  mass,  $M$ , the total width,  $\Gamma_t$ , the partial widths,  $\Gamma_{\pi^+\pi^-J/\psi}$  and  $\Gamma_l$ , the energy spread of the machine, and the non-resonant hadronic cross section.

As the branching fraction of  $\psi(2S)$  to  $e^+e^-$  is small, the cross section for the  $e^+e^-$  final state is dominated by the QED process. Therefore this channel is used to calculate the integrated luminosity at each energy point by an iterative method. First, all  $e^+e^-$  events within  $|\cos\theta| \leq 0.72$  are taken as “Bhabha” events and used to calculate the integrated luminosity at each energy point. A maximum likelihood fit is performed to the observed cross sections for hadron,  $\pi^+\pi^-J/\psi$ , and muon pair final states, and a group of  $\psi(2S)$  parameters is obtained with the assumption of  $e$ - $\mu$ - $\tau$  universality. Then, separating the  $e^+e^-$  events into a QED part, a resonance part and their interference, the integrated luminosity for each energy point is recalculated using the QED part only, and the fitting procedures are redone to get new values for the  $\psi(2S)$  parameters. The iterative process is repeated until the value of the integrated luminosity at each energy point is consistent for two successive iterations.

The fitted curves are shown along with the scan points in Fig. 6. The fitted mass of the  $\psi(2S)$  is corrected to the PDG value [30]. The errors in the other parameters caused by this correction are negligible. The fitted spread in the center-of-mass energy of the machine is  $(1.298 \pm 0.007)$  MeV, in agreement with the expectation ( $\sim 1.3$  MeV). The resultant  $R$  ratio for the hadronic cross section near the  $\psi(2S)$  resonance is  $2.15 \pm 0.16$ , which agrees well with the earlier BES  $R$  measurements [15].

The results of the fit for decay widths and branching fractions are given in Table 4, together with corresponding PDG [30] values for comparison. The errors are the sum in quadrature of statistical, fitting, and systematic uncertainties, including those from acceptance uncertainties, luminosity uncertainties, and a center-of-mass energy uncertainty of 0.10 MeV [32]. The system-

Table 4  
Results and comparison with the PDG2002 [30].

Value	BES	PDG2002
$\Gamma_t(\text{keV})^\dagger$	$264 \pm 27$ (10.1%)	$300 \pm 25$ (8.3%)
$\Gamma_h(\text{keV})$	$258 \pm 26$ (10.1%)	
$\Gamma_{\pi^+\pi^-J/\psi}(\text{keV})^\dagger$	$85.4 \pm 8.7$ (10.1%)	
$\Gamma_l(\text{keV})^\dagger$	$2.44 \pm 0.21$ (8.8%)	$2.19 \pm 0.15$ (6.8%) <sup>‡</sup>
$\mathcal{B}_h(\%)$	$97.79 \pm 0.15$ (0.16%)	$98.10 \pm 0.30$ (0.31 %)
$\mathcal{B}_{\pi^+\pi^-J/\psi}(\%)$	$32.3 \pm 1.4$ (4.4%)	$30.5 \pm 1.6$ (5.2 %)
$\mathcal{B}_l(\%)$	$0.93 \pm 0.08$ (8.5%)	$0.73 \pm 0.04$ (5.5%) <sup>‡</sup>

Note : <sup>†</sup> indicates directly fitted values while others are derived quantities; <sup>‡</sup> indicates the PDG values for  $\Gamma_e$  and  $\mathcal{B}_e$ . The numbers in parenthesis denote the relative errors.

atic error for  $\Gamma_t$ ,  $\Gamma_{\pi^+\pi^-J/\psi}$  and  $\Gamma_l$  is (2.24 – 4.7) %, 3.2 % and (6.4 – 7.0) %, respectively. The correlation coefficients between directly fitted parameters obtained from the fitting are utilized in the calculation of the errors of indirectly determined parameters such as  $\Gamma_h$  and branching fractions. For  $\mathcal{B}_h$ ,  $\mathcal{B}_{\pi^+\pi^-J/\psi}$ , and  $\mathcal{B}_l$ , the uncertainty related to the common error from the luminosity measurement cancels out.

As a check of the fitting procedure,  $\mathcal{B}_{\pi^+\pi^-J/\psi}$  was also determined by a simpler approach. In this approach, the distribution of  $N_h^{obs}$  versus energy was fit with the shape determined from  $N_{\pi^+\pi^-J/\psi}^{obs}$  versus scan energy plus a polynomial to represent the continuum process to determine the number of hadrons coming from  $\psi(2S)$  decays. Using the ratio of the total number of  $N_{\pi^+\pi^-J/\psi}^{obs}$  events corrected by their detection efficiency and the number of  $\psi(2S)$  hadronic decays corrected by their detection efficiency, we directly determine  $\mathcal{B}_{\pi^+\pi^-J/\psi}$ , which agrees very well with the result from the full fitting procedure.

The assumption that lepton pairs couple to the  $\psi(2S)$  only via an intermediate photon [31] im-

plies the existence of the decay  $\psi(2S) \rightarrow \gamma \rightarrow$  hadrons with a branching fraction:

$$\Gamma_{\gamma h}/\Gamma_t = R\Gamma_\mu/\Gamma_t = 0.0199 \pm 0.0019,$$

which corresponds to a width  $\Gamma_{\gamma h}$  of  $5.26 \pm 0.32$  keV.

The  $\psi(2S)$  lepton width  $\Gamma_l = (2.44 \pm 0.21)$  keV obtained in this measurement agrees with the BES previous value of  $\Gamma_e = (2.07 \pm 0.32)$  keV [8], within the error. In addition, this is the first direct measurement to the decay width of  $\psi(2S) \rightarrow \pi^+\pi^-J/\psi$ , and the precision of  $\mathcal{B}_{\pi^+\pi^-J/\psi}$  is much better than previous measurements and the current PDG value.

## Acknowledgments

We gratefully acknowledge the efforts of the staffs of the BEPC accelerator and the computing center at the Institute of High Energy Physics, Beijing. This work is supported in part by the National Natural Science Foundation of China under contracts Nos. 19991480,10175060 and the Chinese Academy of Sciences under contract No. KJ 95T-03(IHEP); and by the Department of Energy under Contract Nos. DE-FG03-92ER40701 (Caltech), DE-FG03-93ER40788 (Colorado State University), DE-AC03-76SF00515 (SLAC), DE-FG03-94ER40833 (U Hawaii), DE-FG03-95ER40925 (UT Dallas).

## REFERENCES

1. G. S. Abrams et al., Phys. Rev. Lett. **33**, 1453 (1974).
2. V. Lüth et al., Phys. Rev. Lett. **35**, 1124, (1975).
3. G. S. Abrams et al., Phys. Rev. Lett.**34**, 1181 (1975).
4. E. Hilger et al., Phys. Rev. Lett. **35**, 625 (1975).
5. R. Brandelik et al., Z.Phys.**C1**, 233 (1979).
6. T. A. Armstrong et al., Phys. Rev. Lett. **68**, 1486 (1992); Phys. Rev. **D47**, 772 (1993).
7. T. A. Armstrong et al., Phys. Rev. **D55**, 1153 (1997).
8. J.Z.Bai et al. ,Phys. Rev. **D57**(1998)3854

9. M. Ambrogiani et al., Phys. Rev. **D62** (2002) 032004-1.
10. B. Aubert et al., Phys. Rev. **D65** (2002) 031101(R).
11. B. Aubert et al., Phys. Rev. Lett. **86**, 2515 (2001).
12. J. Z. Bai et al., Nucl. Instr. Meth. **A458** (2001) 627;  
J. Z. Bai et al., Nucl. Instr. Meth. **A344** (1994) 319;  
J. Z. Bai et al., HEP & NP **16** (1992) 769 (in Chinese).
13. The track momenta are required to satisfy the following requirements:  
$$\tilde{p}_1 \geq 0.95, \text{ or } \tilde{p}_2 \geq 0.95, \text{ or}$$
$$\sqrt{(\tilde{p}_1 - 1)^2 + (\tilde{p}_2 - 1)^2} < 0.16,$$
for an  $e$ -pair, where  $\tilde{p}$  is the normalized momentum:  $\tilde{p} = p/E_{beam}$ . For a  $\mu$ -pair, the corresponding cut is:  
$$P\text{-cut.1} \cap ( P\text{-cut.2} \cup P\text{-cut.3} )$$
where  $P\text{-cut.1}$ ,  $P\text{-cut.2}$ , and  $P\text{-cut.3}$  are defined as following:  
$$P\text{-cut.1: } \sqrt{\left(\frac{\tilde{p}_1 - \tilde{p}_2}{0.35}\right)^2 + \left(\frac{\tilde{p}_1 + \tilde{p}_2 - 1.68}{0.125}\right)^2} > 1,$$
$$P\text{-cut.2: } (\tilde{p}_1 \geq 0.9) \cap (\tilde{p}_2 \geq 0.7),$$
$$P\text{-cut.3: } (\tilde{p}_2 \geq 0.9) \cap (\tilde{p}_2 \geq 0.7).$$
These momentum cuts are shown in Fig. 2.
14. J. Z. Bai et al., Phys. Rev. Lett. **88** (2002) 101802.
15. J. Z. Bai et al., Phys. Rev. Lett. **84**, (2000) 594.
16. J. Z. Bai et al., Phys. Rev. **D58** (1998)092006.
17. BHABHA and MUPAIR were written by F.A.Berends et al. and S. Van der Mark, respectively, and were based on F. A. Berends et al., Nucl. Phys. **B57** (1973) 381; **B68** (1974) 541; **B177** (1981) 237; **B228** (1983) 537.
18. J. C. Chen et al., Phys. Rev. **D62** (2000) 034003-1.
19. X. R. Qi et al., HEP & NP **23** (1999) 1 (in Chinese).
20. J. Z. Bai et al., Phys. Rev. **D62**, (2000) 032002.
21. J. Z. Bai et al., Phys. Rev. **D65** (2002) 052004-1.
22. F. Porter, "Scale Correlation in a  $\chi^2$  Fit", (2002) unpublished.
23. CERN Libaray "MINUIT Reference Manual" version 92.1(March 1992).
24. J. Z. Bai et al., Phys. Lett. **B335**(1995) 374.
25. E. A. Kuraev and V. S. Fadin, Sov.J. Nucl. Phys. **41**(1985)466,  
F. Z. Chen et al., HEP & NP **14** (1990) 585 (in Chinese).
26. G. Altarelli and G. Martinelli, Yellow Report CERN **86-02** (1986) 47;  
O. Nicrosini and L. Trentadue, Phys. Lett. **B196**(1987)551.
27. W. Beenakker et al., Nucl. Phys. **B349** (1991) 323.
28. F. A. Berends and G. J. Komen, Phys. Lett. **B63**(1976)432.
29. T. S. Tsai, SLAC-PUB-3129 (1983);  
J. P. Alexander et al., Nucl. Phys. **B320** (1989) 45.
30. Particle Data Group, K. Hagiwara et al., Phys. Rev. **D66** (2002)010001.
31. L. Köpke and N. Wermes, Phys. Rep. **74**(1989)67.
32. C. Zhang et al., HEACC'92 Hamburg, XVth Int. Conf. on High Energy Accelerators, Hamburg, Germany, July 20 24, 1992, ed. J.Rossbach, p.409.

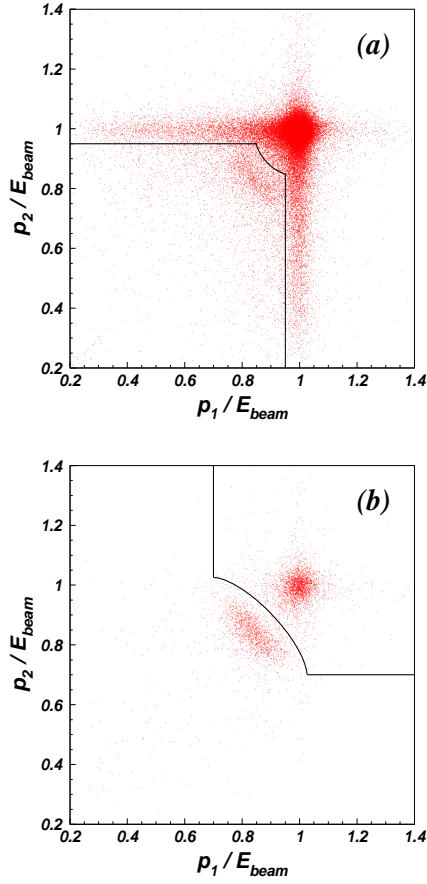


Figure 2. Momentum distributions for (a)  $e^+e^-$  events and (b)  $\mu^+\mu^-$  events. The solid line indicates the cuts applied to remove background from  $\psi(2S) \rightarrow XJ/\psi$ ,  $J/\psi \rightarrow l^+l^-$  [13].

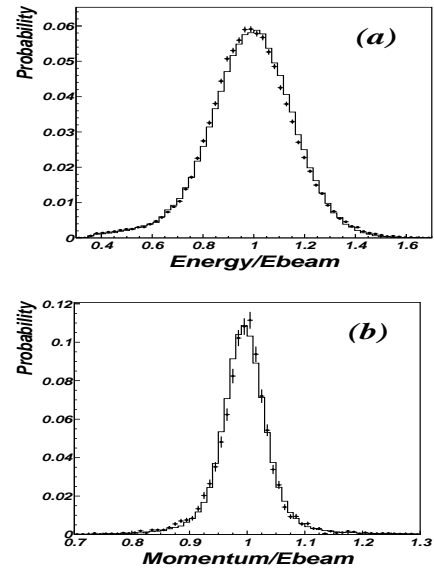


Figure 3. Normalized momentum distributions for (a)  $e^+e^-$  events and (b)  $\mu^+\mu^-$  events. (Histogram for Monte Carlo events and dots with error bar for data)



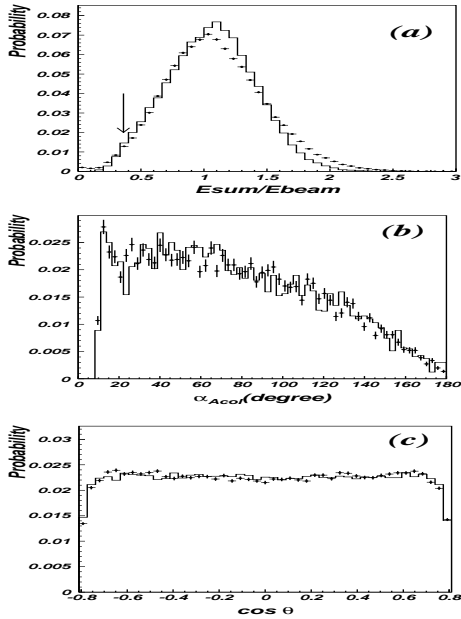


Figure 4. Comparison between Monte Carlo events (histogram) and data (dots with error bar) for hadron events. (a)  $E_{sum}$  (b)  $\alpha_{Acol}$  (c)  $\cos \theta$  of charged track. (The arrow in (a) indicates the cut applied.)

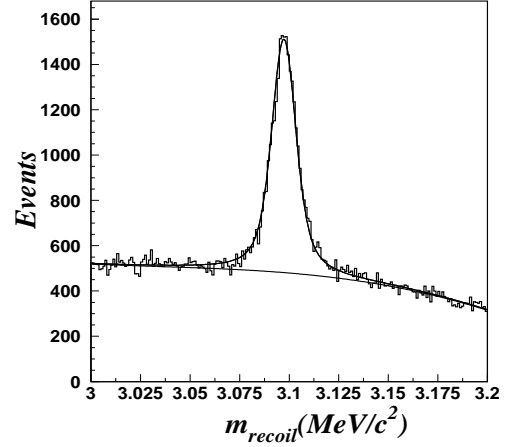


Figure 5. Mass recoiling against  $\pi^+\pi^-$  for all 24 energy points combined. The  $J/\psi$  peak is due to the signal  $\psi(2S) \rightarrow \pi^+\pi^- J/\psi$ ,  $J/\psi \rightarrow$  anything events.

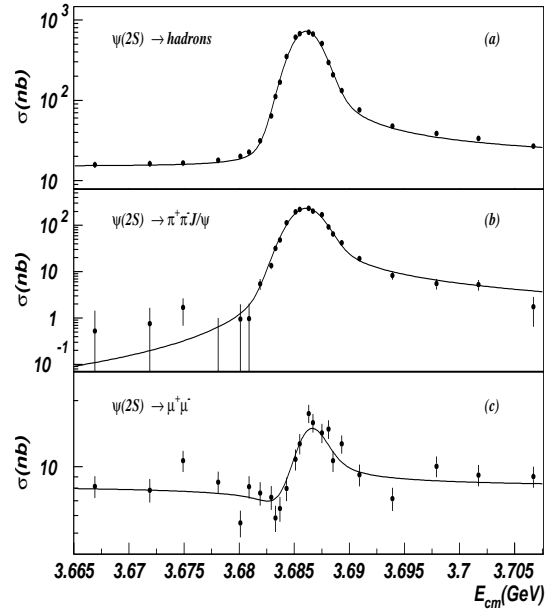


Figure 6. The cross section for (a)  $e^+e^- \rightarrow$  hadrons, (b)  $e^+e^- \rightarrow \pi^+\pi^- J/\psi$ , and (c)  $e^+e^- \rightarrow \mu^+\mu^-$  versus center-of-mass energy. The solid curves represent the results of the fit to the data.